Formation and Structure of Self-Assembled Silica Nanoparticles in Basic Solutions of Organic and Inorganic Cations

Joseph M. Fedeyko, Dionisios G. Vlachos,* and Raul F. Lobo*

Center for Catalytic Science and Technology, Department of Chemical Engineering, University of Delaware, Newark, Delaware 19716

Received December 20, 2004. In Final Form: March 21, 2005

The phase behavior of silica solutions containing organic and inorganic cations was studied at room temperature using conductivity, pH, and small-angle scattering experiments. A critical aggregation concentration (cac) was observed at ∼1:1 ratio of SiO_2/OH^- for all cation solutions from conductivity and pH studies. From this cac, a phase diagram of the system was developed with three distinct phase regions in pseudoequilibrium: a monomer/oligomer region (I), a monomer/oligomer/nanoparticle region (II), and a gel region (III). Small-angle X-ray and neutron scattering (SAXS and SANS) on solutions of region II formed with tetrapropylammonium hydroxide (TPAOH) revealed that the nanoparticles have a core−shell structure. Structure analysis of the SAXS and SANS data was best fit by a core−shell oblate ellipsoid model. A polydisperse set of core−shell spheres also fit the data well although with lower agreement factors. Similar nanoparticle morphologies were found in solutions of TMAOH, CsOH, and NaOH.

Introduction

The development of novel silica materials with a well-defined microstructure, such as zeolites and mesoporous silicas such as MCM-41, has received much attention from the scientific community in recent years.[1,2] To this end, a quantitative understanding of the self-organization of silica would be of great help, yet important aspects of the mechanisms of silica condensation remain unknown. As an example, the role of silica nanoparticles in the formation of zeolite materials, frequently observed prior to and during growth, is still under intensive debate.[3−9] Therefore, despite progress, synthesis of new materials remains an empirical process frequently performed by trial and error.[10,11] A unifying aspect linking the formation of both microporous and mesoporous silica is the interactions between water and silica in the initial stages of the synthesis. According to Iler,[12] in aqueous solutions with a pH above 10, it is easy to form supersaturated silica solutions (compared to the solubility of amorphous silica). Here, we investigate the formation and structure of these solutions at relatively high silica concentrations.

In a previous report,[13] we showed that, in the presence of symmetric organic cations, such as tetrapropylammonium (TPA), a critical concentration of silica exists at which the homogeneous solution suddenly shifts from containing primarily monomer species to a solution containing nanoparticles as well. The formation, stability, and structure of silica nanoparticles are relevant to the homogeneous solution synthesis of silicalite-1, the siliceous form of ZSM-5, which crystallizes in the presence of the TPA cation. Many groups have shown that, in the first phase of the synthesis process, nanoparticles form within the synthesis mixture.[5−8] The importance of these particles on the mechanism for silicalite-1 growth, however, is not well-understood,[7,9,14−16] but their presence in the reaction solutions throughout the growth process suggests that they play some role in the formation of the crystalline solid.

This study focuses on answering two main questions regarding the formation of these nanoparticles. The first question is whether the formation of nanoparticles occurs solely in the presence of tetraalkylammonium (TAA) cations or whether there is a set of experimental conditions at which the nanoparticles form for many cations. We present results for sodium, cesium, tetramethylammonium (TMA), and TPA hydroxide solutions. The second issue is the determination of the shape and structure of these nanoparticles, a crucial step in understanding their stability. As previously shown,[17] temperature and initial

* To whom correspondence should be addressed. E-mail: vlachos@che.udel.edu (D.G.V.); lobo@che.udel.edu (R.F.L.). Phone: 302-831-2830 (D.G.V.); 302-831-1261 (R.F.L.).

(1) Cundy, C. S.; Cox, P. A. *Chem. Rev.* **2003**, *103*, 663.
(2) Davis, M. E. *Zeolites: A Refined Tool for Designing Catalytic Sites* (International Zeolite Symposium) **1995**, 35.
(3) Yang, S. Y.; Navrotsky, A. *Chem. Mater.* **2004**, *16*, 3682.
(4) Knight, C. T. G.; Kinrade, S. D. *J. Phys. Chem. B.* **2002**, *106*, 3329.
(5) Ravishankar, R.; Kirschhock, C. E. A.; Knops-Gerrits, P. P.; Feijen, E. J. P.; Grobet, P. J.; Vanoppen, P.; De Schryver, F. C.; Miehe, G.; Fuess, H.; Schoeman, B. J.; Jacobs, P. A.; Martens, J. A. *J. Phys. Chem. B.* **1999**, *103*, 4960.
(6) Watson, J. N.; Iton, L. E.; White, J. W. *Chem. Commun.* **1996**, *24*, 2767.
(7) Schoeman, B. J. *Microporous Mesoporous Mater.* **1998**, *22*, 9.
(8) Dokter, W. H.; Van Garderen, H. F.; Beelen, T. P. M.; Van Santen, R. A.; Bras, W. *Angew. Chem., Int. Ed. Engl.* **1995**, *34*, 73.
(9) Nikolakis, V.; Kokkoli, E.; Tirrell, M.; Tsapatsis, M.; Vlachos, D. G. *Chem. Mater.* **2000**, *12*, 845.
(10) Davis, M. E.; Zones, S. I. *Abs. Pap. Am. Chem. Soc.* **1995**, *209*, 18.
(11) Zones, S. I.; Davis, M. E. *Curr. Opin. Solid State Mater. Sci.* **1996**, *1*, 107.
(12) Iler, R. K. *The Chemistry of Silica*; John Wiley & Sons: New York, 1979.
(13) Fedeyko, J. M.; Rimer, J. D.; Lobo, R. F.; Vlachos, D. G. *J. Phys. Chem. B* **2004**, *108*, 12271.
(14) Yang, S. Y.; Navrotsky, A.; Wesolowski, D. J.; Pople, J. A. *Chem. Mater.* **2004**, *16*, 210.
(15) Kirschhock, C. E. A.; Buschmann, V.; Kremer, S.; Ravishankar, R.; Houssin, C. J. Y.; Mojet, B. L.; van Santen, R. A.; Grobet, P. J.; Jacobs, P. A.; Martens, J. A. *Angew. Chem., Int. Ed.* **2001**, *40*, 2637.
(16) Cundy, C. S.; Forrest, J. O.; Plaisted, R. J. *Microporous Mesoporous Mater.* **2003**, *66*, 143.
(17) Kragten, D. D.; Fedeyko, J. M.; Sawant, K. R.; Rimer, J. D.; Vlachos, D. G.; Lobo, R. F.; Tsapatsis, M. *J. Phys. Chem. B* **2003**, *107*, 10006.

10.1021/la0468390 CCC: $30.25
Published on Web 04/30/2005

composition can have a significant impact on particle morphology which may explain the diverging particle shape models proposed by other groups[5,8,18] for these particles. We focus on the analysis of nanoparticles synthesized at room temperature from TPA and TMA solutions.

Here, we are able to answer these questions using microstructural information gained from small-angle scattering measurements. We find that not only are these particles present in both basic organic and inorganic solutions but also the conditions of stability and particle morphology are relatively insensitive to the identity of the cations. Using a combination of pH, conductivity, small-angle X-ray scattering (SAXS), small-angle neutron scattering (SANS), and contrast matching experiments, we show that the polymerization of silica in basic solutions is a highly organized process, with a rich and complex phase behavior, and should be understood before we can rationally design functional materials. These observations are in contrast to the general view of silica polymerization as a classical polymerization process giving rise to a broad distribution of molecular structures.

Analysis of Small-Angle Scattering Data

The intensity, $I(q)$, determined in a small-angle scattering experiment is a function of multiple variables containing information about the interactions, structure, and shape of particles and is given by[19] eq 1:

$$I(q) = \Phi V^2(\rho_{\text{particle}} - \rho_{\text{solvent}})^2 P(q)\, S(q) \qquad (1)$$

Here, Φ is the particle volume fraction, ρ is the scattering length density (SLD), V is the particle volume, $P(q)$ is the particle's form factor, and $S(q)$ is the structure factor of the nanoparticle ensemble. The particle volume fraction and the difference in the scattering length density between the particle and the solvent depend on the particle and solution composition and are independent of the particle shape and other structural features. In SANS, the SLD of a particle can be determined through contrast matching experiments using mixtures of deuterated/hydrogenated solvents.[19] Information about the particle shape is included in the form factor, $P(q)$, which describes the scattering from the object, and in the particle volume, V. The effects of interparticle interactions are contained within the structure factor, $S(q)$. For dilute solutions as the ones studied here, particle interactions can be assumed to be negligible ($S(q) = 1$).[19]

For a system of monodisperse, uniform-density particles, eq 1 can be applied directly with $P(q)$ fitted using one of the various available particle shape models and $S(q)$ fitted to various interparticle force models ranging from hard spheres to charged particles in an electrolyte solution. We consider sphere, cylinder, and ellipsoid models for particle shape (i.e., $P(q)$), and the structure factor is modeled using the Hayter–Penfold mean spherical approximation. This model determines $S(q)$ for systems of charged spherical particles in a dielectric medium and can be modified to account for deviations from sphericity.[20]

To explore possible polydispersity, both $P(q)$ and $S(q)$ must be averaged over a distribution of particle sizes, according to

$$P(q) = \int F(q,r)^2\, h(r)\, \mathrm{d}r \qquad (2)$$

Gaussian and rectangular distributions of spherical particles are employed to determine the polydispersity through the weighting function, $h(r)$. The form factor, $F(q,r)$, for a spherical particle is defined as

$$F(q,r) = \frac{4\pi}{3} r^3(\rho_{\text{particle}} - \rho_{\text{solvent}}) \times \left(3\frac{\sin(qr) - qr\cos(qr)}{(qr)^3}\right) \qquad (3)$$

For spatially nonuniform particles, which have an internal distribution of SLDs, the overall form factor is determined through the addition of terms accounting for scattering from the different density regions of the particle.[21,22] The silica nanoparticles are simulated as core–shell shapes (spheres, ellipsoids, and cylinders) with a final $P(q)$ comprised of terms for the core and shell scattering.

In addition to the direct analysis of $P(q)$ and $S(q)$ from reciprocal space data, it is also possible to study small-angle scattering data in real space through the application of the pair distance distribution function (PDDF or $p(r)$), which is the inverse Fourier transform of the scattering function. The distance distribution function represents the averaged density distribution of the particle in space according to the probe radiation. $p(r)$ allows for the analysis of particle shape as well as polydispersity.[23] In addition to the shape information, the determination of $p(r)$ enables the calculation of the particle radius of gyration, R_g

$$R_g^{\,2} = \frac{\int p(r) r^2\, \mathrm{d}r}{2\int p(r)\, \mathrm{d}r} \qquad (4)$$

which for our purposes is the main metric for comparing the differences between SAXS data collected at different solution conditions.[24] R_g has the advantage of being model independent.

Materials and Methods

Silica Solution Preparation. Silica nanoparticle solutions are prepared by first diluting or dissolving the hydroxide form of the desired cation (NaOH, 98.7%, Fisher Chemicals), cesium hydroxide (CsOH, 50 wt % solution in H_2O, Aldrich), tetra-*n*-propylammonium hydroxide (TPAOH, 40 wt % solution in H_2O, Alfa Aesar), and tetramethylammonium hydroxide (TMAOH, 25 wt % solution in H_2O, Alfa Aesar) with deionized water. After stirring for 30 min in a closed Teflon vessel, tetraethyl orthosilicate (98%, Aldrich) is added to yield a final composition (molar ratio) of 9 OH^-:9500 H_2O:x SiO_2:4x EtOH. These solutions are stirred in a closed Teflon vessel for a minimum of 12 h before being analyzed. For neutron scattering studies, the nanoparticle solutions are prepared with 40% TPAOD in deuterated water. TPAOD (40 wt %) is synthesized by mixing TPABr (Aldrich) with deuterated water and silver oxide (Aldrich) in a 1.5:1 molar excess of silver oxide and stirring for 3–5 days. For the solid–liquid equilibrium studies, solutions of varying NaOH, CsOH, TPAOH, and TMAOH concentrations were prepared in the same manner with molar ratios of 4.5 or 29 OH^-:9500 H_2O. The remainder of the composition space was tested with TPAOH and TMAOH at molar ratios of 14, 18, and 40 OH^-:9500 H_2O.

(18) Watson, J. N.; Iton, L. E.; Keir, R. I.; Thomas, J. C.; Dowling, T. L.; White, J. W. *J. Phys. Chem. B.* **1997**, *101*, 10094.
(19) Feigin, L. A.; Svergun, D. I. *Structure Analysis by Small-Angle X-ray and Neutron Scattering*; Plenum Press: New York, 1987.
(20) Hansen, J. P.; Hayter, J. B. *Mol. Phys.* **1982**, *46*, 651.
(21) Arleth, L.; Pedersen, J. S. *Phys. Rev. E* **2001**, *63*, 061406.
(22) Nagao, M.; Seto, H.; Shibayama, M.; Yamada, N. L. *J. Appl. Crystallogr.* **2003**, *36*, 602.
(23) Pedersen, J. S. *J. Appl. Crystallogr.* **1993**, *1994*, 595.
(24) Glatter, O. *J. Appl. Crystallogr.* **1979**, *12*, 166.

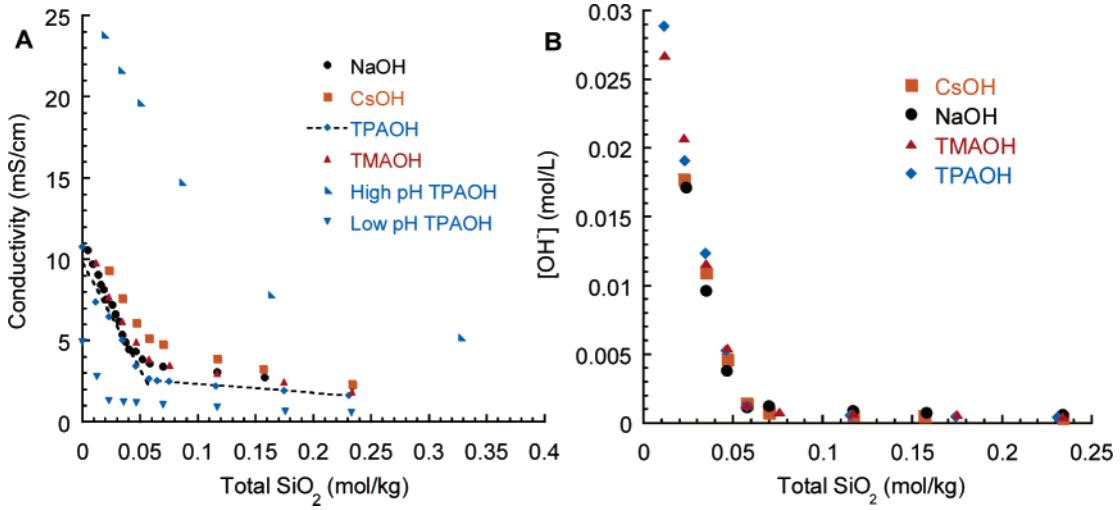

Figure 1. Determination of cac in organic and inorganic cation solutions. (A) Conductivity as a function of total silica concentration. All curves display a sudden change in slope at approximately a 1:1 SiO_2/OH^- molar ratio. After the cac, the slope is related to the ionic mobility of the cation. Variations in initial pH cause shifts of the cac to the corresponding 1:1 SiO_2/OH^- molar ratio. (B) Hydroxide concentration $[OH^-]$ as a function of total silica concentration for organic and inorganic cations. The slope change is independent of cation type and occurs at approximately the same point as that shown in the conductivity measurements.

Analytical Methods. The conductivity of the solutions is measured with a VWR model 2052 EC meter, and pH is measured using a Corning 355 pH/ion analyzer and a Corning high-performance electrode with an Ag-ion barrier. The pH meter was calibrated with standardized pH 10 and 12 buffer solutions (Alfa Aesar). The conductivity meter was tested on KCl standards at three different conductivity values (111, 12.8, 1.40 mS/cm) covering the entire conductivity range of the samples.

SANS measurements were conducted on the 30 m instrument (NG3) at the National Institute of Standards and Technology at Gaithersburg, MD. Samples were prepared following the above methods with D_2O replacing water to increase the contrast between the background and the nanoparticles. The samples were placed in quartz cells of 4 mm path length. A constant neutron wavelength of 6 Å was used with a 2.2 m sample-to-detector distance. Software provided by NIST[25] was used for the normalization of the data and the subtraction of the sample holder scattering. SAXS experiments were conducted on a SAXSess camera SAXS system (Anton-Parr). Samples were placed in a vacuum-tight 1 mm diameter quartz capillary holder and measured at 25 °C. Cu Kα radiation ($\lambda = 1.54$ Å) was used with a 265 mm sample-to-detector distance. The scattering patterns were collected on a phosphor imaging plate in the q range 0.08−8 nm^{-1}. Patterns were normalized to the height of the primary beam signal using the SAXSquant software. Desmearing was conducted by subtracting the signal from a normalized deionized water sample. Reciprocal space scattering patterns were fit using Igor Pro and a shape specific least-squares fitting algorithm (see ref 26). Both SAXS and SANS patterns were further analyzed using the generalized indirect fourier transform (GIFT) version 5-2000 software.[27] The subtracted scattering patterns were fit with a form factor followed by indirect Fourier transform to obtain pair distance distribution functions.

Contrast matching SANS experiments were conducted by varying the ratio of H_2O to D_2O in the final solution. Five contrast points are used at 25, 50, 62, 89, and 100% D_2O. At each point, the absolute intensity, $I(0)$, at $q = 0$ is determined. The square root of $I(0)$ is proportional to the scattering contrast between the particle and the solvent,[19] so if $I(0)^{1/2}$ versus $(\rho_{particle} - \rho_{solvent})$ is plotted, the point of zero contrast for the particle can be determined. This point is referred to as the scattering length density of the particle.

(25) http://www.ncnr.nist.gov/dva/index.html (data reduction web site, NIST Center for Neutron Research).
(26) Kline, S. NIST SANS fitting procedures for Igor Pro. 2001.
(27) Glatter, O.; Fritz, G.; Brunner-Popela, J.; Weyerich, B. GIFT for Windows, 1999.

Results and Discussion

Critical Aggregation Concentration in the Presence of Inorganic Cations. The conductivity and pH (Figure 1) of silica solutions has been followed in the presence of Na^+ and Cs^+ cations at compositions y [Cs^+/Na^+]:9500 H_2O:x SiO_2:4x EtOH, where $y = 4.5$, 9, and 29 and $0 < x < 145$, the same conditions used in ref 13 for symmetric organic cations. Overall, two regions are seen: at low silica concentrations, the conductivity and $[OH^-]$ drop considerably with increasing SiO_2, whereas at high silica concentrations, only slight changes occur. For an initial OH^-/H_2O ratio of 9:9500 at low concentrations of silica, the solution consists of monomers and small oligomers of silica in the protonated ($Si(OH)_4$) and deprotonated ($Si(OH)_3O^-$) forms and ions of OH^-, (Na^+/Cs^+/TPA^+, etc.), and H^+.[28] We refer to oligomeric silica as silica species not large enough to cause measurable scattering in SAXS patterns. It is known from NMR studies that under similar conditions only small oligomers are present.[29]

Although, all the charged species contribute to the conductivity of solution, OH^- is the most significant species because of its high mobility and concentration. The consumption of OH^- ions, through the deprotonation of silica with increasing fraction of silica, is therefore the cause for the drastic decrease in the solution conductivity and pH in the first region of the curves.

$$Si(OH)_4 + OH^- \leftrightarrow Si(OH)_3O^- + H_2O \qquad [R_1]$$

In the second regime, the consumption of OH^- slows down with increasing fraction of silica.

By dividing the curves into two different regions and fitting the linear portion of the curves, a critical aggregation concentration (cac) of the solution can be determined. Particles are observed by SAXS only after this cac has been crossed (see below). The cac values calculated from both conductivity and pH curves (see below) are between 0.047 and 0.058 mol/kg, which represent a variation in the [TEOS]/$[OH^-]$ ratio from 0.89:1 to 1.09:1 for Cs^+ to

(28) Kinrade, S. D.; Knight, C. T. G.; Pole, D. L.; Syvitski, R. T. *Inorg. Chem.* **1998**, *37*, 4272.
(29) Kinrade, S. D.; Knight, C. T. G.; Pole, D. L.; Syvitski, R. T. *Inorg. Chem.* **1998**, *37*, 4278.

rectangular distribution for the polydispersity. We apply the same definition for the polydispersity, which is the standard deviation of the distribution divided by the average particle radius, as the NIST fitting software.[26] In fact, both the core−shell cylinder and ellipse are better fits than the polydisperse core model, although the polydisperse core−shell model is an improvement over the sphere models.

To exclude the possibility of significant nanoparticle polydispersity, a simultaneous analysis of SAXS and SANS patterns was used. We use the polydispersity of the particle's core as the key factor to establish if the polydisperse model is physically feasible, since the particle's shell should remain of constant radius if only a monolayer of TPA^+ adsorbs onto the surface of the particles.[36,37] The core polydispersity determined for both the SANS and SAXS patterns should be nearly the same. For the SAXS pattern, the PDDF of a Gaussian distribution of spherical objects can be determined by summing over the individual PDDF curves of analytical spheres[24] multiplied by the fraction of particles predicted to have a given radius from the Gaussian distribution. The maximum of the experimental PDDF is used as the center of the Gaussian distribution with the standard deviation optimized to yield the best fit to the experimental data. The best fit to the SAXS data gives a mean particle size of 18.3 Å and a standard deviation of 3.6 Å, which yields a polydispersity of 0.20 significantly different from that predicted from the simulation of the SANS patterns. We have tested further the effect of polydispersity following procedures developed for microemulsions[21,22] and found that applying a Gaussian distribution of core sizes to the SANS pattern yielded approximately the same final solution as the fitting procedure with an average core radii of 16 Å and a polydispersity of 0.4. We thus conclude that the overall best fit to the SAXS and SANS patterns is the monodisperse oblate ellipsoid, though more rigorous modeling may validate a polydisperse or cylindrical solution that is consistent with the experimental data.

Figure 8 displays the final fitted SANS pattern including the minor effects of the Hayter−Penfold approximation for the structure factor. The Hayter−Penfold approximation assumes a sample of uniform spherical particles that have a net charge, e^- (electrons). It is possible to use this structure factor for nonspherical particles using the decoupling approximation, as recently shown by Bergstrom for tablet shaped particles.[38] The scattering cross section, $d\sigma(q)/d\Omega$, in the decoupled case is defined as

$$\frac{d\sigma(q)}{d\Omega} = (\rho_{particle} - \rho_{solvent})^2 M \langle F^2(q)\rangle_0 \times \left(1 + \frac{\langle F(q)\rangle_0^2}{\langle F^2(q)\rangle_0}(S(q) - 1)\right) \quad (5)$$

where M is the molecular mass of the nanoparticle. The structure factor for the nanoparticles was analyzed using eq 5 with an oblate ellipse model for the form factor with varying aspect ratios ranging from spheres to very thin platelike particles. The inclusion of particle shape (last term in eq 5) only led to small deviations in the simulated structure factor when compared to the basic Hayter−Penfold model. Consequently, we have used the Hayter−Penfold structure factor for spherical particles with an effective diameter based on the form factor parameters to include interparticle force effects in the simulation of the scattering patterns.[26]

Figure 8. Experimental and fitted SANS patterns of TPA nanoparticles using core−shell models. A structure factor including the effects of electrostatic forces between TPA nanoparticles is added to the best fit particle shape solution (the oblate core−shell ellipsoid) capturing the low q characteristics of the SANS pattern.

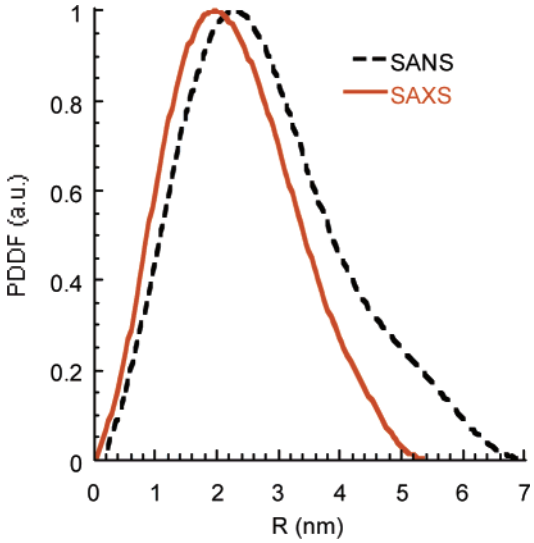

Figure 9. Neutron and X-ray PDDFs for TMA nanoparticles. The TMA nanoparticle displays the same core−shell structure observed for the TPA nanoparticle.

We performed the same structural analysis for nanoparticles formed with TMAOH and found similar final results. As with the TPAOH nanoparticle, SAXS and SANS measurements can be described well by a core−shell particle structure (Figure 9). Complete analysis of the SANS scattering patterns yielded an oblate ellipse as the best fit for the nanoparticle core with a major radius of 30 Å and in line with a SAXS fit of 28 Å. The optimal shell thickness is a thinner layer than that possible for a layer of TMA^+. This difference may be due to multiple factors including surface roughness and particle density gradients, both of which will require more detailed models.

(36) Tetraalkylammonium cations have been shown to form aggregates in water solutions but only at molarities (1 mol/L)[29] well above those in our studies (0.052−0.35 mol/L), so we do not expect multilayers or TAA^+ aggregates in the system to affect polydispersity.

(37) Wen, W.; Saito, S. *J. Phys. Chem.* **1964**, *68*, 2639.
(38) Bergstrom, M.; Pedersen, J. S. *J. Phys. Chem. B.* **1999**, *103*, 8502.

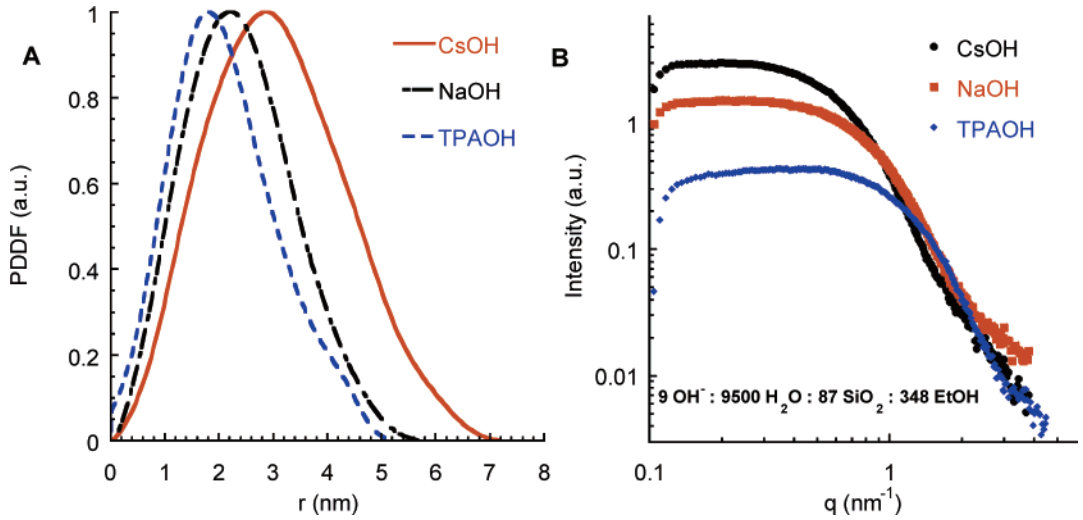

Figure 10. Particle morphology of inorganic cation nanoparticles. (A) PDDFs of the SAXS patterns. Cs and Na particles appear to have a larger particle size than TPA in SAXS patterns. The PDDF shape indicates the particles are not spherical. (B) SAXS pattern of nanoparticles of Cs^+, Na^+, and TPA^+. The PDDFs indicate variations in the nanoparticle size between the three cations as well as concentration differences.

The PDDF of the SAXS and SANS patterns demonstrate conclusively that there is a TMA^+ layer surrounding the particle.

Microstructure of the Nanoparticles in the Presence of Inorganic Cations. We have shown through the comparison of SAXS and SANS patterns that silica–TPA nanoparticles have a core–shell structure with silica in the core and TPA^+ mostly in the shell. Analysis of TMA^+ solutions displays this same core–shell particle structure. However, it remains to be determined whether these observations can be extended to inorganic cations.

The SAXS patterns for Na^+, Cs^+, and TPA^+ solutions (Figure 10A) show a distinct peak at nearly the same q value, while an IFT[27] analysis of the PDDFs calculated from these SAXS patterns (Figure 10B) with compositions of 9 R^+OH^-:9500 H_2O:40 SiO_2:160 EtOH indicates that all particles are similar (elongated shapes) but with slightly different sizes. We attempted to verify the size of the particles with SANS for the Na^+OD^- system; the analysis of the scattering data indicates that the particles have an ellipsoidal shape with dimensions similar to that obtained from the SAXS patterns. Further analysis was not possible due to the relatively weak scattering signal. Note that, unlike TPA^+ and TMA^+, the X-ray scattering contrast between the Na^+ and Cs^+ ions and water is a factor of 10 higher (1.1×10^{-7} Å^{-2} for TPA^+ and -1.51×10^{-6} Å^{-2} for Na^+). Even with the inclusion of a hydration sphere of water surrounding the Na^+ ion, the contrast is 5 times greater, allowing for the nanoparticle shell to be observed in SAXS. Consequently, inorganic cations should be easily observed in the SAXS patterns. For instance, the R_g calculated from these PDDFs increases from 15 Å for TPA^+ to 23.5 Å for Cs^+ (see Table 2). A comparison of the SAXS PDDF in Figure 10B with the SANS PDDF of TPAOH (Figure 11) is revealing. Both the TPAOH and CsOH PDDFs have the same maximum value. The only difference between the two is a slight increase in nanoparticle size in the TPAOH case which can be attributed to the large cation size. The similarity of these two PDDF patterns and macroscopic behavior of the solutions strongly indicate that the Cs and TPA particles have the same core–shell structure.

Summary and Conclusions

The formation of silica nanoparticles at room temperature has been studied in both inorganic and organic strong base solutions. For all strong base solutions studied here and in our previous report,[13] a critical point for nanoparticle formation (cac) has been shown to exist at ~1:1 SiO_2/OH^- ratio. Prior to this critical point, no nanoparticles are detected in solution, and the addition of small amounts

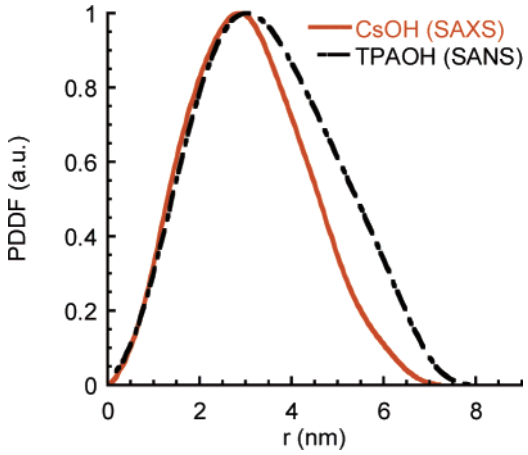

Figure 11. Comparison of Cs nanoparticle X-ray PDDF with TPA nanoparticle neutron PDDF. The apparent increase in particle size displayed in the SAXS pattern is caused by the increase in cation scattering cross section. For Cs, the surface cation layer is observed in the SAXS pattern leading to a similar PDDF distribution as a SANS pattern of a TPA nanoparticle where the surface cation layer is also visible. The larger size for the TPA nanoparticle is related to the difference in size between the two cations.

Table 2. Summary of Critical Aggregation Concentrations and Nanoparticle Radii of Gyration

Initial composition	cac from [OH^-] (mol of SiO_2/kg)	cac from conductivity (mol SiO_2/kg)	R_g (Å)
9 TMAOH:9500 H_2O	0.058	0.052	17.7
9 TPAOH:9500 H_2O	0.056	0.054	14.9
9 NaOH:9500 H_2O	0.055	0.047	18.3
9 CsOH:9500 H_2O	0.058	0.055	23.5
29 TPAOH:9500 H_2O	0.176	0.185	8.8
4.5 TPAOH:9500 H_2O	0.024	0.024	20.1
4.5 TMAOH:9500 H_2O	0.028	0.034	20.4
4.5 NaOH:9500 H_2O	0.026	0.027	19.5
4.5 CsOH:9500 H_2O	0.022	0.029	20.4
29 TMAOH:9500 H_2O	0.181	0.184	8.7
29 NaOH:9500 H_2O	0.181	0.182	32.5
29 CsOH:9500 H_2O	0.17	0.196	29.6

of silica monomer in the form of TEOS only results in the deprotonation of $Si(OH)_4$, as was previously known.[12] After the cac, silica condensation leads to charged nanoparticles with an oblate ellipsoidal shape as the best fit of our data. These particles show a pseudoequilibrium phase behavior with three distinct regions: a monomer/oligomer region prior to the cac, a monomer/oligomer/nanoparticle region after the cac, and a gel region at high SiO_2/OH^- ratios. Nanoparticle formation is reversible through suitable addition or removal of SiO_2 or OH^-. Within the nanoparticle region, the particle size appears to be closely linked to the initial concentration of OH^- in solution.

Acknowledgment. This work was funded by the National Science Foundation under Grant No. 0103010. We acknowledge Stephen Ekatan for his assistance with the TMAOH experiments and David Kragten and Jeff Rimer for their assistance in gathering the SANS data. The X-ray experiments were made with a SAXSess small-angle X-ray instrument on loan from Anton Paar GmbH, in Graz/Austria. This work utilized facilities supported in part by the National Science Foundation under Agreement No. DMR-9986442. We acknowledge the support of the National Institute of Standards and Technology, U.S. Department of Commerce, in providing the neutron research facilities used in this work.

LA0468390